JOURNAL OF PROPULSION AND POWER
Vol. 17, No. 3, May–June 2001

Influence of Compressor Exit Conditions on Combustor Annular Diffusers Part II: Flow Redistribution

A. G. Barker* and J. F. Carrotte†
Loughborough University, Loughborough, England LE11 3TU, United Kingdom

In gas-turbine engines the velocity of air, issuing from the compressor, must be reduced in order to permit effective operation of the downstream combustor. This is partly achieved by locating an annular diffuser behind the compressor outlet guide vanes (OGVs) and, in modern systems, the inlet of this diffuser is usually located at the trailing edge of the blade row. This paper is concerned with some of the interactions that occur between these components and, in particular, the flow redistribution that occurs along the diffuser length due to the flows generated by the OGV blade passage and upstream rotor. A mainly experimental investigation has been undertaken, on a fully annular facility, which incorporates a single-stage axial flow compressor and simulated flame tube. In addition, immediately downstream of the OGV row a constant-area passage, or diffusers of area ratio 1.45 or 1.60, can be incorporated. The OGV blade row produces a profile that, as a result mainly of the blade wakes, contains an excess of kinetic energy relative to that of a uniform profile. The mixing out of these wakes therefore enhances the pressure rise within the downstream diffuser. Measured mean velocity data are used to determine the path of streamlines along each diffuser and indicate regions where high-energy fluid is being convected, toward each casing, and low-energy boundary layer fluid is being removed. This is because of the remnants of the flows generated within each OGV passage. The mean momentum equation along each diffuser is then used to indicate that such flows significantly offset the changes in momentum, within each boundary layer, that are associated with the applied pressure gradient. Such effects are therefore thought significant in terms of reducing the boundary-layer growth and delaying flow separation from the casings.

Nomenclature

A	=	passage area
AR	=	area ratio
C	=	OGV blade chord
Cp	=	static pressure rise coefficient
h	=	annulus passage height
L	=	diffuser length
m	=	mass flow
P, p	=	local stagnation, static pressure
Rn	=	nondimensional radius $[(r - r_i)/(r_o - r_i)]$
r	=	radius relative to rig centerline
r_i, r_o	=	inner-casing, outer-casing radius
s, n, z	=	coordinates relative to the local inviscid streamline (see Fig. 3)
T	=	temperature
U, V, W	=	velocity components for x, r, θ coordinate system (see Fig. 3)
U_s, V_s, W_s	=	velocity components for s, n, z coordinate system (see Fig. 3)
x, r, θ	=	coordinates relative to the rig centerline (see Fig. 3)
α	=	kinetic energy flux coefficient based on the overall profile
α_r	=	kinetic energy flux coefficient based on the average radial profile
λ	=	stagnation pressure loss coefficient
$\bar{}$	=	mass-weighted spatial mean value

Subscript

0, 1, 2	=	OGV inlet, diffuser inlet, and diffuser exit traverse planes

Received 21 February 2000; revision received 9 July 2000; accepted for publication 9 July 2000.

*Research Assistant, Rolls-Royce University Technology Centre.
†Rolls-Royce Lecturer in Aerospace Propulsion, Rolls-Royce University Technology Centre.

Introduction

IN gas-turbine engines the velocity of air, issuing from the compression system, must be reduced in order to permit effective operation of the downstream combustor. This is partly achieved by locating a diffuser immediately behind the compressor outlet guide vane (OGV) blade row. Optimization of engine performance means maximizing the velocity reduction within this diffuser, while maintaining a stable flow, prior to the flow undergoing an abrupt expansion as it enters the combustion system. This is the second of two papers that are concerned with the aerodynamic interaction which occurs between the annular diffuser and the axial compressor stage which is located immediately upstream.

In Part I the numerous diffuser investigations that are relevant to the gas-turbine application were reviewed. These included investigations with axisymmetric boundary-layer-type inlet conditions or, alternatively, investigations in which more representative inlet conditions were provided by an upstream compressor. In general it was noted that greater pressure rises were achieved, relative to those indicated by diffuser performance charts, when the inlet conditions were provided by an upstream compressor. This agreed with the results that were presented in Part I, which defined the overall performance of several diffusers that were located downstream of a single-stage axial flow compressor. Detailed analysis indicated that the inlet profile provided to each diffuser contained a relatively large amount of kinetic energy because of the presence of wakes from the compressor OGVs. Despite the pressure forces introduced by the diffusing passage the high shear forces, associated with the blade wakes, ensured that these circumferential distortions decreased, thereby leading to a relatively high diffuser pressure rise. However, whereas the results in Part I explained the origins of the increased pressure rise, no explanation was provided as to how these higher pressure gradients were sustained by the boundary layers, adjacent to each casing, so that flow separation was avoided. Work by previous authors has suggested that, in addition to the mean-flow distribution at the diffuser entrance plane, the enhanced turbulence provided by the compressor can improve spanwise mixing and thereby reduce boundary-layer growth and the onset of separation. With this in mind, it is thought investigations into the spanwise mixing and redistribution of high loss fluid that occurs within axial-compressor blade rows may also

be of relevance. For example, Adkins and Smith,[1] Gallimore and Cumpsty,[2] Wisler et al.,[3] and Leylek and Wisler[4] have all investigated both secondary flow and turbulent diffusion as mechanisms for the spanwise and cross-passage mixing in axial flow compressors, the relative importance of these mechanisms depending on configuration and loading levels.

Whereas the Part I paper concentrated on the overall performance of the OGV/diffuser system, this paper (Part II) attempts to establish what potential mechanisms, generated by the upstream blade row, are responsible for reducing the growth of the casing boundary layers and delaying separation. Such effects enable the low-energy bounday-layer fluid to remain attached to each casing despite the increased pressure gradient along the diffuser. Results are therefore presented that were obtained using the same single-stage axial flow compressor and diffusers that were described in Part I. This included using annular diffusers of the same axial length but which had area ratios of 1.0 (i.e., parallel passage), 1.45, and 1.60. In all tests a flame tube, typical of current gas-turbine engine practice, provided a representative blockage to the flow issuing from these diffusers.

Experimental Facility

A description of the overall experimental facility has already been provided in Part I, with the working section approximating a large-scale version of a current engine (Fig. 1). An 80-blade inlet guide vane (IGV) row precedes the rotor, which is operated at a flow coefficient of approximately 0.4 and a nondimensional speed ($N/\sqrt{T}$) of 170. The mean radius of the IGV, rotor, and OGV blade rows is 375 mm with a passage height of 36.6 mm; at a mass flow of 4.6 kg/s, the mean axial velocity is approximately 45 m/s (Mach number ~0.13). Within the facility various OGV and diffuser geometries can be incorporated while the blockage presented by a downstream flame tube is also simulated.

For the tests reported here the OGV row consisted of 160 controlled diffusion blades of chord 39 mm and 6% thickness/chord ratio, with these blades being typical of current engine hardware. At OGV exit this same blade row could be attached to diffusers of area ratio 1.0 (parallel passage), 1.45, and 1.60 (Fig. 2), with each diffuser having an axial length of 2.23 inlet passage heights (i.e., 2.23 h_1). In addition, the axial length between OGV exit and the flame tube head was also maintained constant at 3.63 h_1. According to the design criteria obtained with the boundary-layer-type flows described by Howard et al.,[5] for a nondimensional length of 2.23 h_1 the diffusers with area ratios 1.45 and 1.60 fall within the attached flow regime.

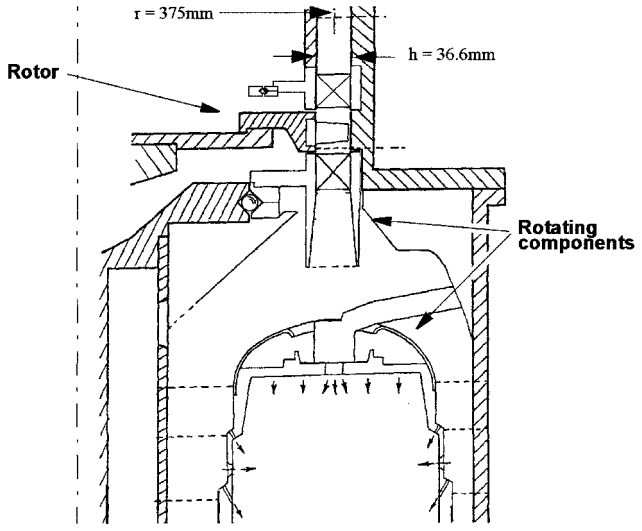

Fig. 1 Test facility.

Instrumentation

For the results presented here, area traverses across two blade spaces were obtained at $x/L = 0.0$, 0.21, 0.43, and 1.0 within each diffuser (Fig. 2). These traverses were performed using miniature five-hole pressure probes of overall diameter 1.5 mm, hole bore 0.25 mm, which were used in a nonnulled mode as outlined by Wray and Carrotte.[6] For each of these traverses some 820 data points were obtained, with 20 radial measurement locations being repeated at 41 circumferential positions. In addition, five-hole probe traverses were performed on the diffuser centerline, midway between blades, at typically 20 positions between OGV exit ($x/L = 0.0$) and the exit of each diffuser ($x/L = 1.0$). These measurements were used to provide information on the static pressure rise along the diffuser centerline. The method by which radial and circumferential movement of the instrumentation was achieved is the same as that outlined in Part I, as are the experimental errors associated with the instrumentation.

Data Reduction

Diffuser Performance

The diffuser performance is assessed from area traverses with five-hole pressure probes, at diffuser inlet and exit, which provide information on stagnation and static pressure in addition to velocity magnitude and direction. For the area traverses this information can be used to derive the overall mean velocity U_m and mass flow through each traverse plane. In addition, mean values of stagnation pressure ($\bar{p}$) were defined by mass weighting the appropriate individual values. For spatially nonuniform incompressible flow, which is in a predominantly axial direction, it also follows that

$$\bar{P} = \bar{p} + \alpha\left(\tfrac{1}{2}\right)\rho U_m^2 \tag{1}$$

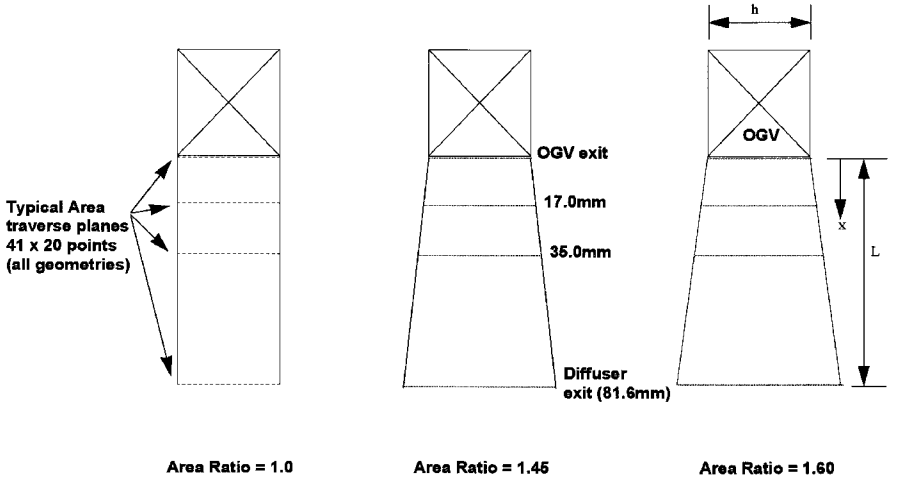

Fig. 2 OGV/diffuser geometries.

in which

$$\alpha = \frac{1}{A}\int_A \left(\frac{u}{U_m}\right)^3 \mathrm{d}A, \qquad \bar{p} = \frac{1}{m}\int_m p\rho u \, \mathrm{d}A$$

where α is the kinetic energy flux coefficient and represents the ratio of mass-weighted mean kinetic energy of a nonuniform flow, to that of a uniform flow with the same mass-flow rate.[7] As in Part I, changes in the spatially averaged pressures between planes 1 and 2 are expressed in terms of a total pressure loss λ and static pressure rise coefficient Cp in which these changes are nondimensionalized by a reference dynamic head.

$$\lambda = (\bar{P}_1 - \bar{P}_2)/(\bar{P} - \bar{p})_1, \qquad C_p = (\bar{p}_2 - \bar{p}_1)/(\bar{P} - \bar{p})_1 \quad (2)$$

Mean Momentum Equation

If effects from curvature are small, then the mean momentum equation for incompressible, steady flow is given by

$$U_s\frac{\partial U_s}{\partial s} + V_s\frac{\partial U_s}{\partial n} + W_s\frac{\partial U_s}{\partial z} = \frac{-1}{\rho}\frac{\partial p}{\partial s} - \left(\frac{\partial}{\partial s}\overline{uu} + \frac{\partial}{\partial n}\overline{uv} + \frac{\partial}{\partial z}\overline{uw}\right) \quad (3)$$

In this nomenclature s, n, z are the coordinates along (s) and normal to (n, z) the direction being considered. The terms on the left-hand side of this equation are associated with the acceleration, undertaken by the fluid, whilst the terms on the right-hand side represent the forces being applied to the element of fluid. These arise as a result of gradients in either pressure or the turbulent stresses, the latter often being dominated by the shear-stress gradients. Such terms can be considered relative to the diffusers being tested. For example the path traced out by a particle as it moves along the length of a diffuser is dictated by the applied pressure and turbulent forces. Alternatively, at a given location the acceleration of the fluid ($U_s\partial U_s/\partial s$), in addition to the applied forces, is also a function of the velocity components and gradients normal to the direction being considered ($V_s\partial U_s/\partial n + W_s\partial U_s/\partial z$).

For practical reasons the area traverses, within each geometry, have been conducted on planes normal to the x direction (Fig. 3). However, if a one-dimensional inviscid flow is considered, then velocity components will be generated, that are normal to the x direction, as a result of the diverging passage. Of interest in this investigation is the movement and redistribution of fluid caused by the flows generated by the upstream blade row. Hence, what must be considered is the momentum equation for the flow passing along these inviscid streamlines (Fig. 3). However, in addition to assuming that curvature effects are small, some simplifications are required, to Eq. (5), because of the alignment of the traverse planes with the local streamlines. For example,

$$V_s\frac{\partial U_s}{\partial n} = V_s\sin\beta\frac{\partial U_s}{\partial x} + V_s\cos\beta\frac{\partial U_s}{\partial r} \approx V_s\cos\beta\frac{\partial U_s}{\partial r}$$

$$\frac{1}{\rho}\frac{\partial p}{\partial s} = \frac{1}{\rho}\frac{\partial p}{\partial x} + \frac{1}{\rho}\frac{\partial p}{\partial r} \approx \frac{1}{\rho}\frac{\partial p}{\partial x}$$

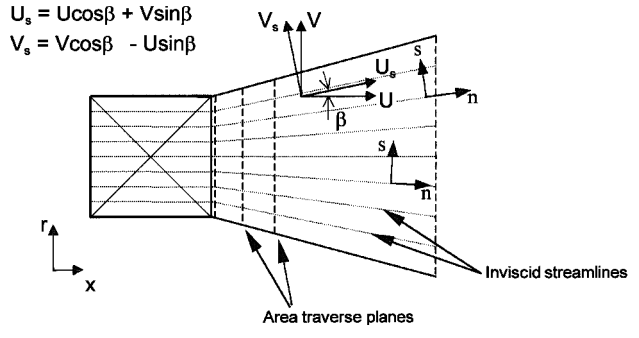

Fig. 3 Diffuser nomenclature.

where these assumptions are justified because 1) β is relatively small (max. value ~7 deg), 2) away from the OGV trailing-edge velocity gradients in the radial direction are much greater than those in the axial direction, and 3) the axial pressure gradient is significantly greater than the radial pressure gradient (because the OGVs ensure the flow is predominantly in the axial direction). Based on these assumptions, the momentum equation (5) that is applied along the inviscid streamlines (Fig. 3) becomes

$$U_s\frac{\partial U_s}{\partial s} + V_s\frac{\partial U_s}{\partial r} + \frac{W_s}{r}\frac{\partial U_s}{\partial \theta} \approx \frac{-1}{\rho}\frac{\partial p}{\partial x} - \left(\frac{\partial}{\partial s}\overline{uu} + \frac{\partial}{\partial n}\overline{uv} + \frac{\partial}{\partial z}\overline{uw}\right) \quad (4)$$

The streamwise and normal velocity components can be calculated from the measured velocity data. In addition, the mean velocity gradients have been derived by fitting a three-term Lagrange polynomial to this data in either the radial or circumferential directions.

Results and Discussion

Inlet Conditions

Whereas Part I was merely concerned with changes to the mean axial velocity distribution within each diffuser, of interest in this paper are the secondary flow features generated by the blade row upstream of each diffuser. The circumferentially averaged profiles of axial velocity, swirl angle, stagnation and static pressures measured at OGV inlet are therefore presented (Fig. 4). At this location the axial velocity profiles indicate the hub and casing boundary layers, each occupying approximately 20% of the passage height, with the swirl distribution indicating a nominal air angle of approximately 45 deg within the central portion of the passage. The rise in stagnation pressure toward the hub is associated with the upstream spinning rotor disc, while rotor-tip clearance effects influence this profile toward the outer casing. Efforts have been made to ensure these conditions are typical of those presented to an OGV row within a modern engine and, within experimental error, these conditions were maintained constant for all the OGV/diffuser geometries tested.

The trailing edge of the OGV blade row is located at inlet to the diffuser ($x/L = 0.0$), and an indication of the overall flow distribution, at this location, is provided by the axial velocity contours for the case with the parallel passage downstream (Fig. 5a). Circumferential variations in the flow field caused by OGV wakes are clearly evident, but the distribution also indicates a relatively well-behaved blade row with no significant regions of flow separation. In addition to the axial velocity contours, flow vectors at the diffuser inlet plane are also presented (Fig. 5b). Unlike tests with more conventional boundary-layer-type inlet conditions components of velocity, which are normal to the mainstream direction, are generated by the upstream blade row. Furthermore, at this location changes in the flowfield, associated with the different downstream geometries, are relatively small. Hence, the assumption can be made that the different pressure fields, associated with each diffuser, have little influence on the flow within the OGV passages, and so this flow distribution (Fig. 5) is representative of the conditions being presented to all three diffuser geometries.

Diffuser Performance

The axial velocity contours, at diffuser exit, for both the area ratio 1.0 (parallel passage) and 1.60 diffusers (Fig. 6) show that for both geometries the flow has remained attached to the casings at all circumferential locations. Also presented is the static pressure distribution measured along the centerline of each diffuser (Fig. 7), whereas the tabulated performance data, presented in Part I, indicated the relatively high overall static pressure rise within each diffuser. As already discussed, the pressure rise is influenced by the OGV blade row, which presents a profile to the diffuser that contains a relatively large amount of kinetic energy. However the steep velocity gradients, and hence high shear stresses, associated with these features ensure that significant mixing out of the wakes occurs downstream of the blade row, and so a rise in pressure ($Cp = 0.130$) is observed

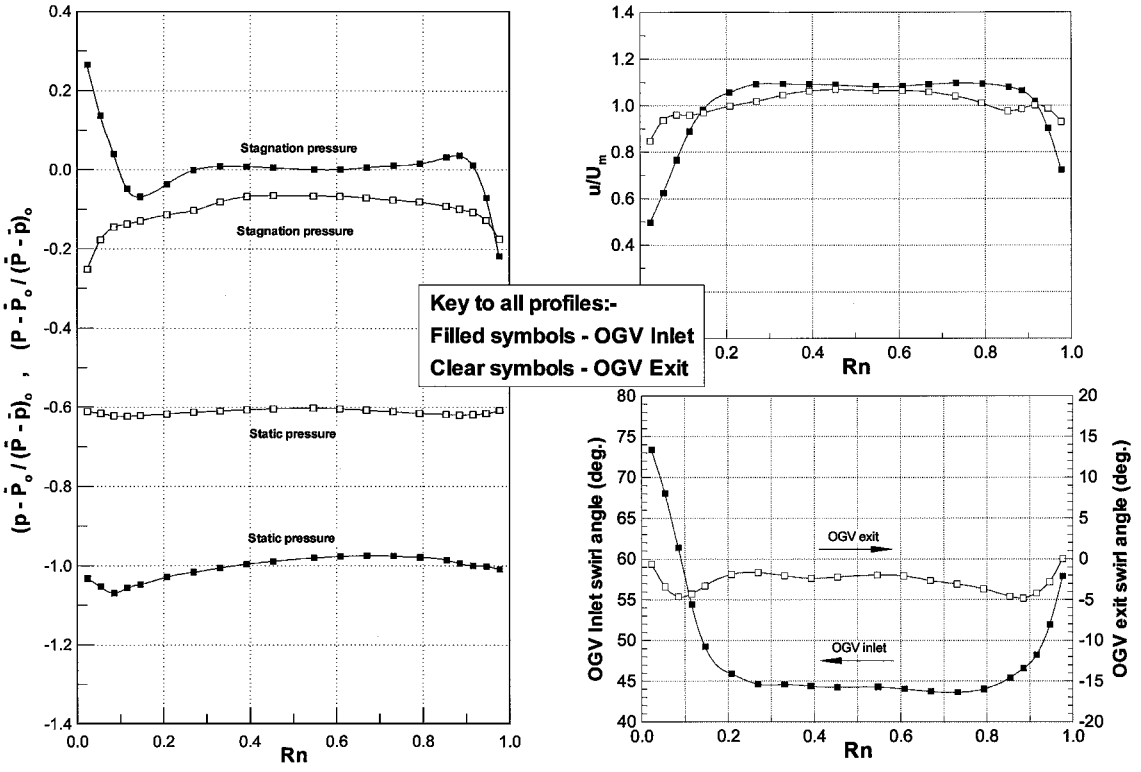

Fig. 4 Circumferentially averaged profiles at OGV inlet and exit.

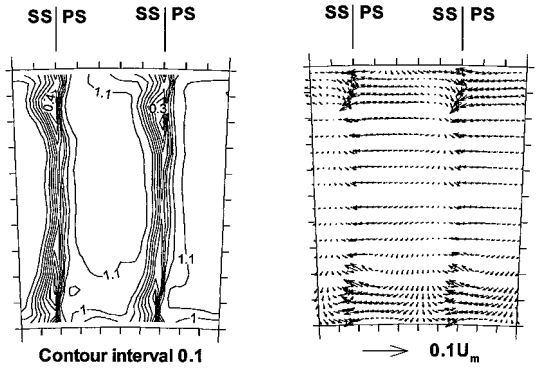

a) Axial velocity contours (U/U_m) **b) Flow vectors**

Fig. 5 Axial velocity contours and flow vectors (OGV exit, area ratio = 1.0).

even within the parallel passage. With increasing area ratio the associated pressure forces suppress, to a limited extent, the blade wake mixing while promoting the growth of low-energy boundary-layer fluid adjacent to each casing. Nevertheless, for all three geometries tested relatively high static pressure increases were observed.

The static pressure rise along each diffuser (Fig. 7) can be compared with that obtained using more conventional axisymmetric inlet conditions with relatively thin inlet boundary layers[8] or a fully developed profile.[5] These data are often in the form of diffuser performance charts which indicate, within a given axial length, the area ratio at which the maximum pressure rise is achieved. At larger area ratios the pressure gradients cannot be sustained, by the casing boundary layers, so resulting in flow separation and a reduction in the diffuser pressure rise. For the current nondimensional length of diffusers being tested, results from Sovran and Klomp[8] and Howard et al.[5] indicate a maximum pressure rise Cp of approximately 0.41. However, the pressure rise within the 1.45 and 1.60 area ratio diffusers far exceeds this value (Fig. 7). Although the reasons for this additional pressure rise have already been explained in Part I, in terms of the inlet profile development within the diffuser, it should be remembered that this increased pressure gradient will be imposed on the casing boundary layers. For all of the geometries tested, though,

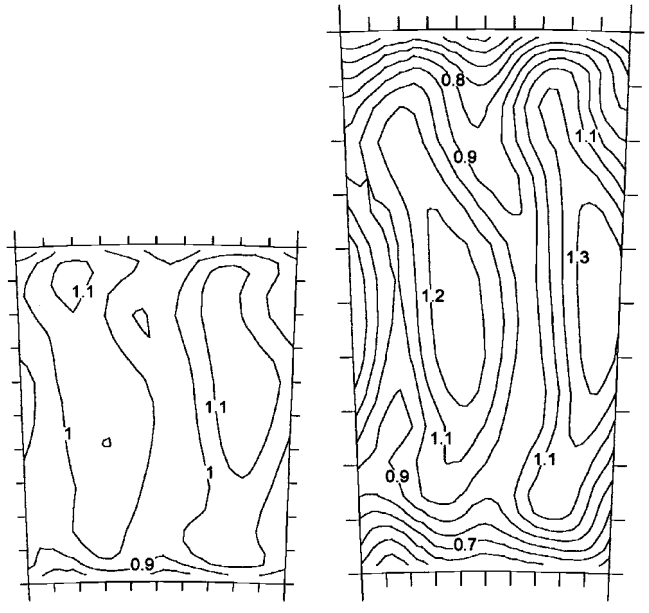

Fig. 6 Axial velocity contours (U/U_m) at diffuser exit (AR = 1.0, 1.60).

the boundary layers are attached to the casings at diffuser exit (Fig. 6), and it must therefore be concluded that the inlet conditions being provided, by the upstream OGV row, enable the low-energy flow adjacent to each casing to sustain this increased pressure rise.

The inlet conditions presented to a diffuser can have a significant impact on its performance. For example, Stevens and Williams[9] obtained performance benefits by placing a coarse grid and spoiler upstream of their diffusers, whereas Klein,[10] in his review article, comments that turbulence generally reduces flow distortions within diffusers and delays separation. It is widely accepted that these benefits are caused by the transmission of turbulent energy toward the diffuser walls, and, with this in mind, the orientation of the turbulent eddies is therefore also important. In the application being considered in this paper, the inlet conditions are generated

by upstream turbomachinery. Hence, this not only generates the highly three-dimensional boundary layers that have already been described (Fig. 6) but flows that are normal to the axial direction. For example, secondary flows can be generated by the pressure forces acting on the flow within each passage while changes to the mean flowfield can also be turbulent in origin, i.e., as a result of turbulent shear stresses associated with radial gradients in velocity. Various authors have considered these processes[1–4] within a blade passage and their importance in redistributing high-loss fluid away from the hub and casings toward the passage center. Whether the spanwise and cross-passage flows within the blade passages originate from secondary flows or turbulent effects has no bearing in this investigation. However, the remnants of these flows, and the turbulence effects that could continue downstream of the blade row, may be of significance in terms of influencing flow development within the diffuser. In particular, these flows are significant in enabling the casing boundary layers to sustain the applied pressure gradient, the magnitudes of which are relatively large as a result of the diffuser inlet profile.

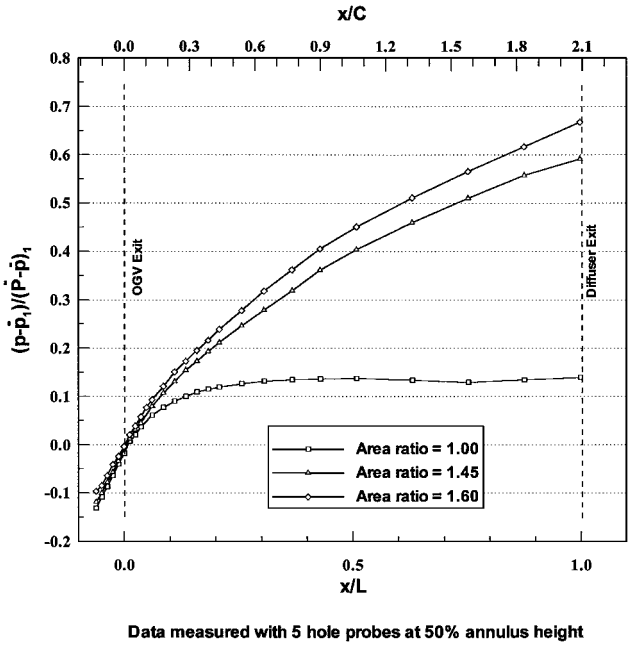

Fig. 7 Static pressure distributions along the diffuser centerlines.

Flow Streamlines

At OGV exit the swirl-angle distribution (Fig. 4) indicates the presence of blade passage flows typical of those generated within compressor blade rows. For example, increasing swirl angles close to the hub and casing (Fig. 4) indicate classical flow overturning, whereas the flow vectors (Fig. 5) clearly indicate velocity components that are normal to the mainstream direction. However the amount of circumferential or radial movement that occurs within the diffuser, as a result of these velocity components, may not be significant because of the relatively large streamwise component. One method by which the fluid redistribution can be assessed is by tracing the path of massless particles within the diffuser passage, this path being defined as the tangent to the local mean-flow vector. The simplest method by which this can be achieved is to assume that the local flowpath is constant until the next traverse plane is intercepted, the flowpath then changing to correspond with the local mean-flow vector at the point of interception. However, in this case a more sophisticated approach was achieved by using the Tecplot v7.5 software package. In this case the local flow direction is interpolated between the experimental traverse planes, with the indicated particle path being tangential to both the experimental and interpolated flow vectors. In theory the path of each streamline is determined by the remnants of the blade-row flows, together with the pressure and shear forces that are applied downstream of the blade row within the diffuser passage. A streamline is shown (Fig. 8) emerging from the OGV exit plane ($x/L = 0.00$), tracing the path of a hypothetical particle to diffuser exit ($x/L = 1.00$). When viewed looking upstream, the three-dimensional streamline is projected onto a two-dimensional sector showing the radial and circumferential movement of the particle as it passes through the diffuser. This technique and method of presentation will be applied to the experimental data.

Mean velocity components were obtained from area traverses performed at $x/L = 0.00$, 0.21, and 0.43 using a five-hole probe. The results presented therefore represent the trajectory taken by particles along the initial 43% of the diffuser length. Starting at OGV exit, some 410 locations were studied, with 41 particles being released

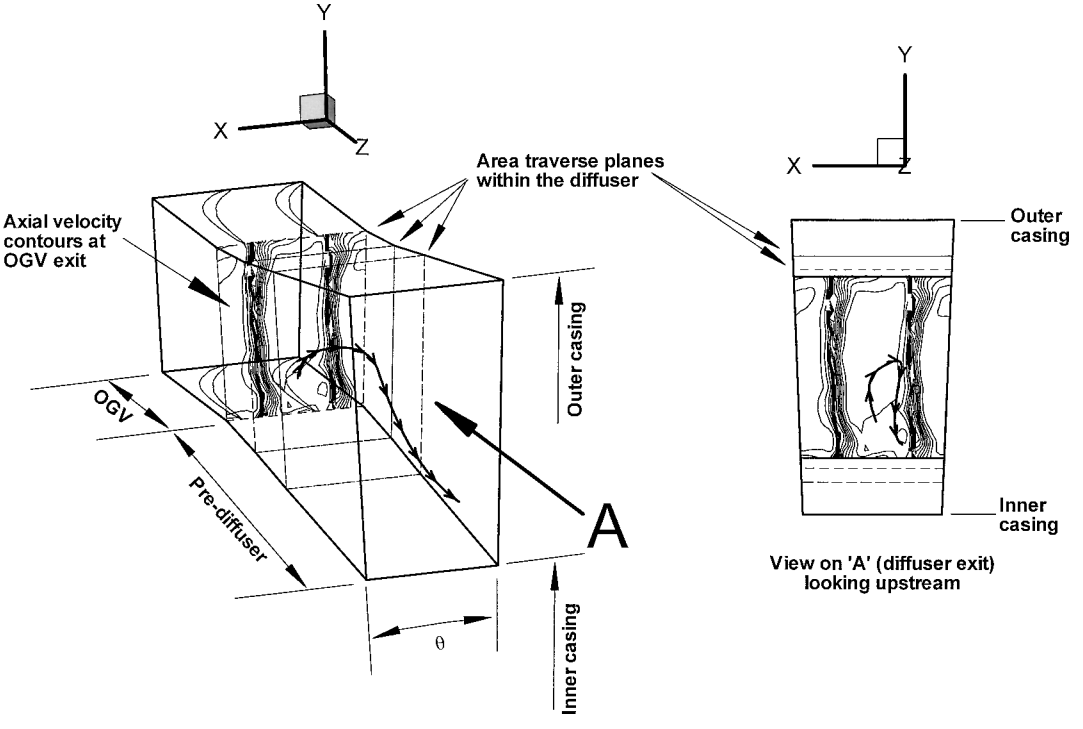

Fig. 8 Three-dimensional view of a particle streamline within the diffuser.

at 10 radial locations. Superimposed on the axial velocity contours at $x/L = 0.00$ (OGV exit) and $x/L = 0.43$, for the parallel passage ($AR = 1.0$) geometry, are these traced particles (Fig. 9). Note the direction of movement can be deduced by remembering that, at OGV exit, the particles were initially released at 10 radial locations only. Furthermore, the streamlines are, of course, the same in each diagram. However, superimposing them on the axial velocity contours at both the start ($x/L = 0.00$) and end ($x/L = 0.43$) planes allows the indicated fluid movement to be compared with the axial velocity development. In particular, a good correlation is observed between the shape of the velocity contours that have developed, between $x/L = 0.00$ and 0.43, and the indicated fluid trajectories (Fig. 9). For example, there is clear evidence of general flow under turning by the OGV blade row, of less than 1 deg, within the central passage region. This is in agreement with the observed circumferential movement of the blade wake, as shown by the axial velocity contours, and the OGV exit swirl-angle distribution. However, it should also be noted that between wakes there is a radial movement of fluid toward the hub and casing as the flow progresses along the passage, accompanied by increased circumferential fluid movement. In contrast, in the immediate vicinity of the wakes the movement of fluid is away from the hub and casing surfaces, toward the center of the passage.

The conditions generated by the OGV row are similar for each of the geometries tested, and so similar effects are likely to be observed within the diffusing passages. In a parallel duct ($AR = 1.0$) the passage flows that are responsible for the radial and circumferential flow redistribution are broadly indicated by the components of velocity normal to the axial direction (V, W). However, for the diffusing case radial velocity (V) components will be generated, even in the absence of secondary flows, as a result of the diverging passage. This is illustrated by the trajectories for the area ratio 1.60 geometry, which have been superimposed on the axial velocity contours at $x/L = 0.0$ and 0.43 (Figs. 10a and 10b). To indicate a relative movement of fluid either toward, or away from, the hub and casing surfaces, the trajectories between $x/L = 0.0$ and 0.43 are therefore presented in terms of their nondimensional location within the diverging passage (Fig. 10c). Note that similar characteristics of radial and circumferential movement of fluid, caused by the secondary flows, are observed as for the $AR = 1.0$ configuration. These similarities suggest that effects associated with the diffuser geometry are not responsible for the observed fluid movement and, instead, it is the flowfield generated within the OGV row. This is further confirmed by the path of each streamline, which, in most cases, is in a similar direction to the local velocity components measured at OGV exit.

The path traced by the streamlines can be considered relative to that expected with more conventional boundary-layer inlet conditions. In such cases the boundary-layer growth would result in a general movement of the streamlines away from each casing and toward the center of the diffuser. With an upstream compressor it appears a mechanism is provided whereby high-energy flow is being convected radially toward the casing boundary layers and swept circumferentially along each surface, while low-energy boundary-layer fluid is being removed from the surface in the vicinity of each wake. However, what cannot be assessed from these traces is how significant this effect is in terms of increasing the momentum in the near-wall regions and helping the casing boundary layers withstand the applied pressure gradient.

Estimate of Momentum Convection

The streamlines indicate a relative movement of flow both toward and, in the vicinity of the blade wake, away from the diffuser casings. However, no quantitative information is provided to indicate if this effect is significant in terms of convecting momentum toward the diffuser walls, thereby reducing boundary-layer growth and delaying the onset of separation. However, at a local point in the flow the convection of momentum can be estimated. For example, the radial and circumferential convection of streamwise momentum is approximately indicated by the terms $V_s \partial U_s/\partial r$ and $W_s/r(\partial U_s/\partial\theta)$, where U_s and V_s are the mean velocity components in the direction of, and normal to, the streamlines that would be present for an inviscid flow (Fig. 3). These terms are approximations but they should, based on order of magnitude arguments, give a reasonable indication of the convection of momentum, both circumferentially and radially, toward each casing surface.

Contours that indicate the convection of momentum, which have been derived from the experimental data, are presented at plane $x/L = 0.21$ (Fig. 11) for the parallel passage and 1.60 area ratio diffuser. Negative values (i.e., grey regions) indicate a net local gain of

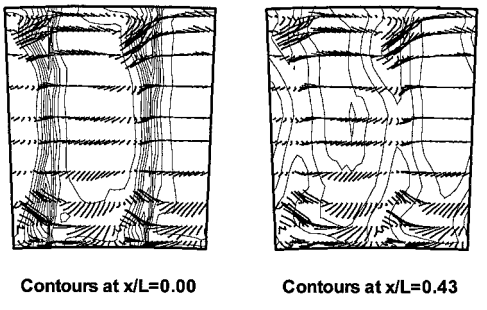

Fig. 9 Axial velocity contours and streamlines (area ratio = 1.00, streamlines 0.00 to 0.43).

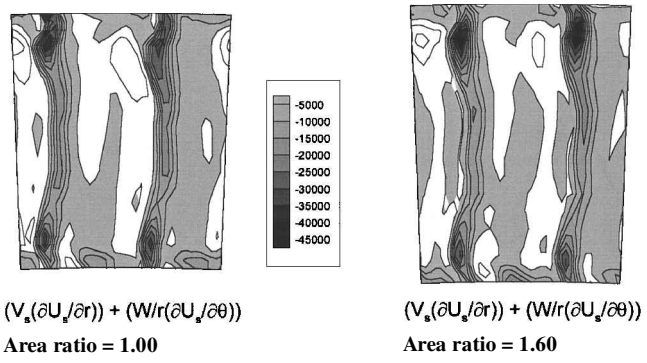

Fig. 11 Radial and circumferential convection of momentum (absolute values at $x/L = 0.21$).

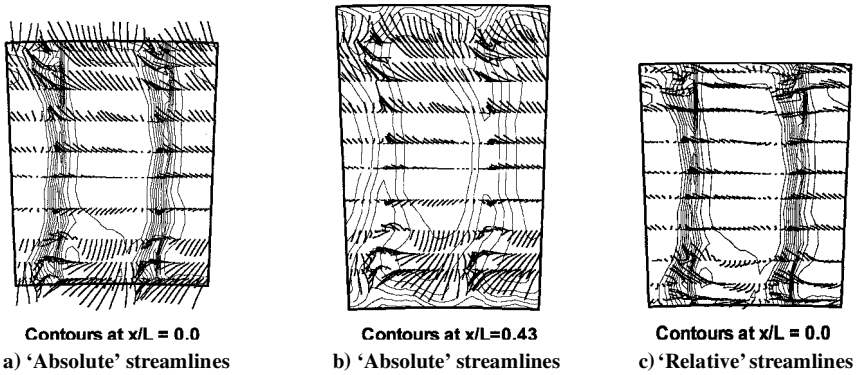

a) 'Absolute' streamlines **b) 'Absolute' streamlines** **c) 'Relative' streamlines**

Fig. 10 Axial velocity contours and streamlines (area ratio = 1.60, streamlines 0.00 to 0.43).

momentum caused by the convection of higher momentum fluid into these regions. In contrast, the white regions indicate those areas of the diffuser passage in which momentum is being convected away. Hence, the circumferential movement of blade wakes, as a result of residual swirl from the upstream blade row, accounts for the large positive and negative regions that span most of the passage height. However, close to the hub and casing local regions, into which momentum is being convected, can be observed while there are other regions, close to each blade wake, into which low-momentum fluid is being convected and higher-momentum fluid removed. Although there are some differences between the contours observed for the parallel passage and 1.60 area ratio diffuser, the overall pattern of fluid movement and redistribution for these configurations is similar. The aforementioned observations are consistent with the particle trajectories already described in which high-energy flow was observed to move radially toward the casing boundary layers and be swept circumferentially along each surface, with low-energy boundary-layer fluid being removed from the surface in the vicinity of each wake.

To assess the significance of these effects, it would be desirable for the calculated values to be expressed relative to the pressure and shear forces that are being applied to the flow at that point. Unfortunately no turbulent information is available, and so, as a compromise, the derived values are expressed relative to the change in momentum associated with the applied pressure force $(1/\rho)(\partial p/\partial x)$, as defined by measurements along the diffuser centerline (Fig. 7). It must be acknowledged that there are regions, particularly close to the diffuser casings, where the turbulent shear forces will be very large. For example, at the casing surface the axial pressure gradient $(\partial p/\partial x)$ will equal the shear force $(\partial \overline{uv}/\partial n)$. Nevertheless, presenting the data in this way at least allows the convection effects to be assessed relative to the pressure gradients associated with the different diffuser area ratios. For the 1.60 area ratio diffuser the contours of the combined radial and circumferential convection of momentum are therefore presented in this way (Fig. 12a[i]). As already presented, grey regions indicate a net local gain of momentum while the white regions indicate those areas of the diffuser passage where momentum is being convected away. By presenting the data in this way it can be seen, for example, close to each casing momentum values are in excess of 50% of the momentum change associated with the applied pressure force. Hence the applied force, caused by the pressure rise, is being offset by the convection of higher-momentum fluid into the boundary-layer regions. By plotting the fluid convection caused by radial flow $(V_s \partial U_s/\partial r)$, the effects of the circumferential blade wake movement can be removed (Fig. 12a[ii]). In general, it can be seen that momentum is being convected away from the central region of the diffuser passage, and, close to the hub and casing, the increase in momentum is being dominated by this radial fluid movement. This can be compared with that expected for conventional boundary-layer-type inlet conditions where the boundary-layer growth, within the diffuser, would generate radial velocity components V_s away from each casing. Hence at a given location there would be a local reduction in momentum caused by the growth of this slow moving boundary-layer fluid (although this is partially offset by turbulent interchange). However, this is the opposite to that observed with the compressor generated inlet conditions, where the convection effects indicate momentum is being increased.

The data presented at diffuser exit (Fig. 12b) indicate how the convection effects vary along the diffuser relative to the applied pressure gradient. Although not presented here, similar trends were also observed within the other geometries tested. It is to be expected that the relative movement of fluid, as a result of the blade passage flows issuing from the OGV row, will be more evident toward the front of the diffuser. Furthermore, it also appears that these effects are more prominent in the hub region. However, as the flow develops downstream the radial convection of momentum toward the outer casing becomes more evident and is particularly pronounced at diffuser exit (Fig. 2b[ii]). Now several workers including Fishenden and Stevens[7] and Carrotte et al.[11] have noted the beneficial effect on a diffuser with a flame tube located downstream. Hence the upstream pressure field from the flame tube is generating radial velocity components causing this effect which, as a result of the flame tube location and

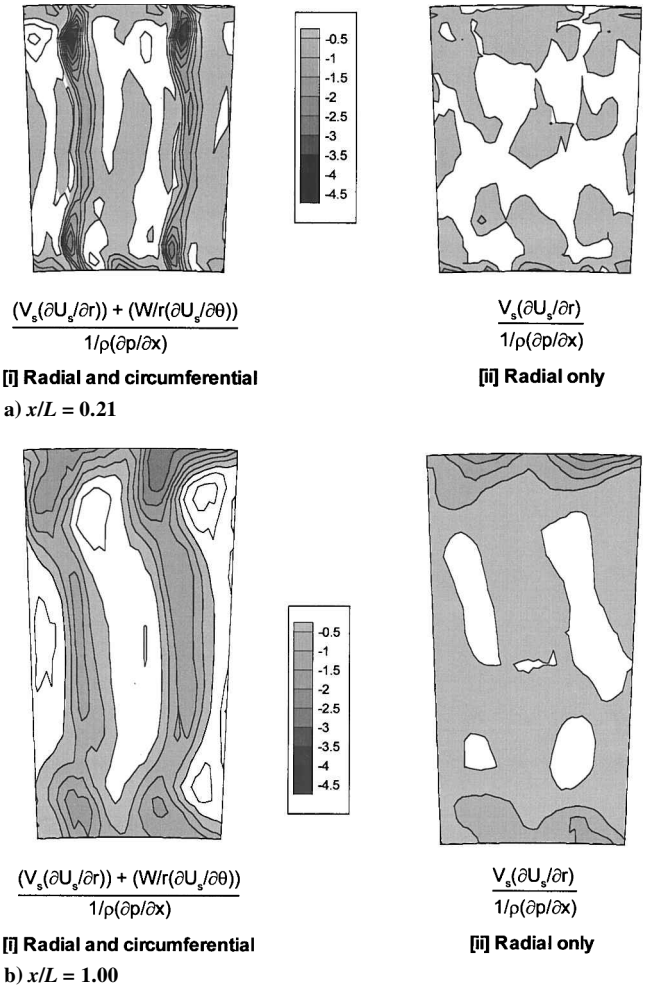

Fig. 12 Radial and circumferential convection of momentum (area ratio = 1.60).

flow distribution around it, means this effect is more pronounced in the outer-casing region. The circumferential variation of this effect is caused by the flow gradients $(\partial U_s/\partial r)$ associated with the blade wakes. However what can also be noted from these data is that this widely accepted process by which the diffuser is stabilized, by the downstream flame tube, is of comparable magnitude to the effects in the early part of the diffuser, which are associated with the compressor generated flowfield.

Conclusions

Measurements have been made behind a single-stage compressor in which, immediately down-stream of the OGV row, the pressure gradient has been varied by using either a parallel passage or diffusers of area ratio 1.45 and 1.60. The OGV blading and diffusers simulate the flows generated within a modern combustor diffuser system and the following conclusions have been drawn:

1) The pressure rise within each diffuser is significantly enhanced by the mixing out of the OGV blade wakes. Diffuser performance charts indicate that such a pressure rise is beyond that which the boundary layers could sustain using more conventional axisymmetric inlet conditions.

2) Streamlines within each diffuser indicate regions where high-energy fluid is being convected toward each casing and low-energy boundary-layer fluid is being removed. Although these streamlines are influenced by the pressure and shear forces within each diffuser, the path of each streamline is predominantly associated with the inlet conditions that are provided by the upstream OGV blade.

3) For the 1.45 and 1.60 area ratio diffusers in excess of 50% of the momentum change associated with the applied pressure forces is being offset by the convection of high-momentum fluid toward

each boundary layer. Hence, these effects are thought significant in terms of reducing the boundary-layer growth and delaying flow separation from the casings.

These measurements have been conducted at the compressor design operating condition and both the mean inlet velocity profile, and these other flow features will vary when the compressor is operated at a different condition. Furthermore, the observed interactions suggest a more integrated approach to the design of the OGV and diffuser components, rather than designing such components in isolation, while the performance should also be quoted on an integrated basis.

Acknowledgments

The authors would like to acknowledge D. Glover, L. Monk, and W. Nivin for their assistance in the manufacture of the test rig and to A. P. Wray for his help in the mechanical design of this facility. In addition, the helpful comments of S. J. Stevens are also greatly appreciated.

References

[1]Adkins, G. G., and Smith, L. H., "Spanwise Mixing in Axial Flow Turbomachines," *Journal of Engineering for Power*, Vol. 104, No. 1, 1982, pp. 97–110.

[2]Gallimore, S. J., and Cumpsty, N. A., "Spanwise Mixing in Multistage Axial Flow Compressors Part I: Experimental Investigation," *Journal of Turbomachinery*, Vol. 108, 1986, pp. 10–16.

[3]Wisler, D. C., Bauer, R. C., and Okiishi, T. H., "Secondary Flow, Turbulent Diffusion, and Mixing in Axial Flow Compressors," *Journal of Turbomachinery*, Vol. 109, 1987, pp. 455–482.

[4]Leylek, J. H., and Wisler, D. C., "Mixing in Axial-Flow Compressors: Conclusions Drawn from 3-D Navier–Stokes Analyses and Experiments," *Journal of Turbomachinery*, Vol. 113, April 1991, pp. 139–160.

[5]Howard, J. H. G., Henseler, H. J., and Thornton-Trump, A. B., "Performance and Flow Regimes for Annular Diffusers," American Society of Mechanical Engineers, Paper 67-WA/FE-21 (A68-11861), June 1967.

[6]Wray, A. P., and Carrotte, J. F., "The Development of a Large Annular Facility for Testing Gas Turbine Combustor Diffuser Systems," AIAA Paper 93-2546, July 1993.

[7]Fishenden, C. R., and Stevens, S. J., "Performance of Annular Combustor-Dump Diffusers," *Journal of Aircraft*, Vol. 14, No. 1, 1977, pp. 60–67.

[8]Sovran, G., and Klomp, E., "Experimentally Determined Optimum Geometries for Rectilinear Diffusers with Rectangular, Conical or Annular Cross-Section," *Fluid Mechanics of Internal Flow*, Elsevier Publ. Co., Amsterdam, 1967, pp. 270–312.

[9]Stevens, S. J., and Williams, G. J., "The Influence of Inlet Conditions on the Performance of Two Annular Diffusers," *Journal of Fluids Engineering*, Vol. 102, No. 3, 1980, pp. 357–363.

[10]Klein, A., "Characteristics of Combustor Diffusers," *Progress in Aerospace Science*, Vol. 31, No. 1, 1995, pp. 171–271.

[11]Carrotte, J. F., Bailey, D. W., and Frodsham, C. W., "Detailed Measurements on a Modern Combustor Dump Diffuser System," *Journal of Engineering for Gas Turbines and Power*, Vol. 117, No. 4, 1995, pp. 678–685.